*Journal of Experimental and Theoretical Physics, Vol. 94, No. 2, 2002, pp. 299–306.*
*Translated from Zhurnal Éksperimental'noĭ i Teoreticheskoĭ Fiziki, Vol. 121, No. 2, 2002, pp. 354–362.*


**SOLIDS**
**Structure**

# Magnetic, Optical, and Electrical Properties of Solid Solutions $V_xFe_{1-x}BO_3$

**N. B. Ivanova, V. V. Rudenko, A. D. Balaev, N. V. Kazak, V. V. Markov, S. G. Ovchinnikov*, I. S. Edel'man, A. S. Fedorov, and P. V. Avramov**

*Kirenskiĭ Institute of Physics, Siberian Division, Russian Academy of Sciences, Akademgorodok, Krasnoyarsk, 660036 Russia*

** e-mail: sgo@iph.krasn.ru*

Received July 2, 2001

**Abstract**—Complex studies of magnetic, electrical, and optical properties of $V_xFe_{1-x}BO_3$ solid solutions are carried out in the entire range of concentrations between the extreme compounds $VBO_3$ and $FeBO_3$. A concentration semiconductor–insulator transition accompanied by a change in the magnetic structure is observed. It is found that the physical properties of the solid solution under investigation differ from those predicted in the model of a virtual crystal in the form of an aggregate of V and Fe centers taken with the weight of $x$ and $1-x$, respectively. The systems of electron energy levels of the $VB_6O_6$ and $FeB_6O_6$ clusters are calculated from first principles using the Hartree–Fock method. The calculated electron structure forms the basis for simulating the optical absorption spectra, which are in good agreement with experimental results. A qualitative explanation is given for the entire body of data on electrical conductivity and magnetization. © *2002 MAIK "Nauka/Interperiodica".*

## 1. INTRODUCTION

Antiferromagnetic dielectric oxides of 3*d* metals have become the objects of intense studies as Mott–Hubbard dielectrics with strong electron correlations. Their alloying leads to the emergence of high-temperature superconductivity in copper oxides and the colossal magnetoresistance effect in manganese oxides. A number of borates $ABO_3$ of 3*d* metals (A = Fe, Cr, V, Ti) form another class of isostructural oxides with strongly differing electrical and magnetic properties [1–3]. Such a difference in the properties is apparently associated mainly with different occupancies of the 3*d* shell, which determines different types of exchange interactions in these compounds. Among these compounds, $FeBO_3$ has been studied comprehensively, while the data on other representatives of this class (especially solid solutions in which the consequences of competing exchange interactions may be manifested most clearly) are exceptionally scarce.

The $VBO_3$ and $FeBO_3$ compounds are, respectively, a ferromagnet ($T_C$ = 32 K) and an antiferromagnet with weak ferromagnetism ($T_N$ = 348 K). At $T$ < 500 K, the former compound is a semiconductor and the latter is an insulator. Both compounds have the same crystal structure of a calcite of the rhombohedral system with the same lattice parameters $a$ = 4.62 Å and $c$ = 14.52 Å, which is apparently due to virtually identical ionic radii of $V^{3+}$ and $Fe^{3+}$ ions. The magnetic properties of $VBO_3$ and $FeBO_3$ are determined by an indirect 90° exchange through the $O^{2-}$ anions; a considerable difference in these properties can be attributed to their different electron configurations ($d^2$ and $d^5$, respectively). The high value of $T_N$ for $FeBO_3$ indicates the high-spin state of the $Fe^{3+}$ ion. The magnetic moment of the $V^{3+}$ ion in $VBO_3$, determined from the saturation magnetization in the ferromagnetic phase, is the sum of the spin and orbital magnetic moments and is approximately 6% lower than the theoretical value. It is unclear whether this discrepancy is a consequence of noncollinearity of the magnetic moments due to the Dzyaloshinski interaction or results from the effect of covalence.

In the present work, we analyze an aggregate of magnetic, electric, and optical properties of $V_xFe_{1-x}BO_3$ solid solutions in the entire concentration range between the extreme compounds.

## 2. SAMPLES AND PREPARATION TECHNOLOGY

Crystals of the mixed composition $V_xFe_{1-x}BO_3$ were grown by spontaneous crystallization from the solution–melt of the system $Fe_2O_3$–$V_2O_3$–$B_2O_3$–(20PbO + 30$PbFe_3$ wt %). We used compositions with the following relation between components:

$$(1-x)Fe_2O_3 - xV_2O_3 = 10\text{–}15 \text{ wt \%}, \quad x = 0.5\text{–}1.0,$$

$$B_2O_3 = 40\text{–}42.5 \text{ wt \%},$$

$$0.2PbO + 0.3PbF_2 = 42.5\text{–}50 \text{ wt \%}.$$

It should be noted that the value $x$ is given in accordance with the concentration of components in the charge and is approximate.

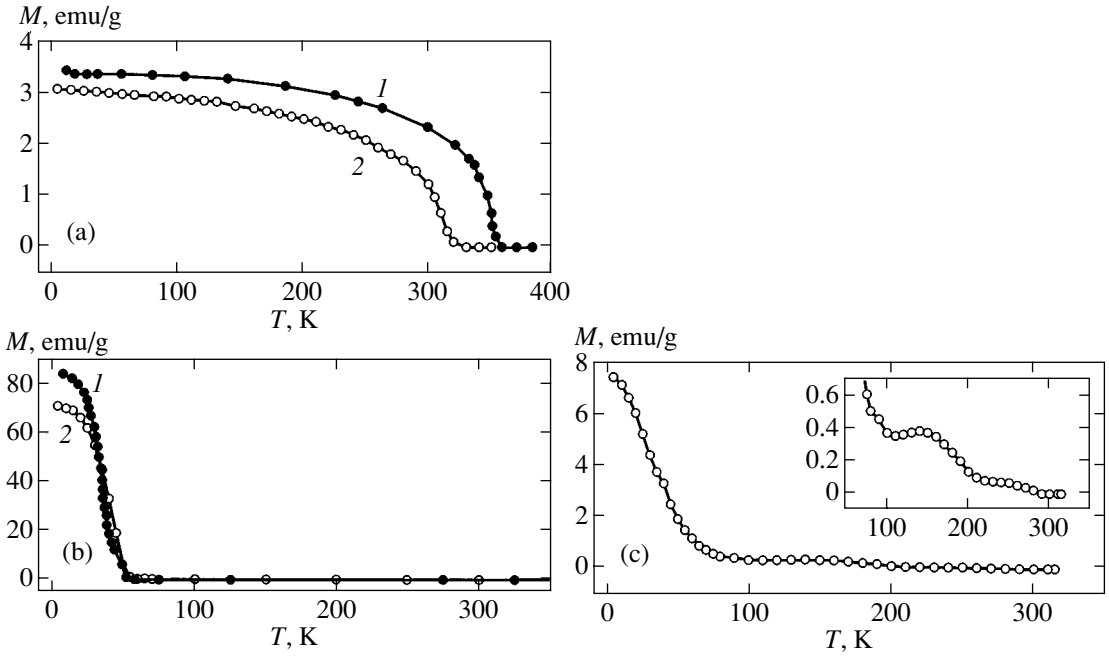


**Fig. 1.** Temperature dependence of magnetization in a magnetic field $H = 10$ kOe: (a) $FeBO_3$ (*1*), $V_{0.5}Fe_{0.5}BO_3$ (*2*); (b) $VBO_3$ (*1*), $V_{0.95}Fe_{0.05}BO_3$ (*2*); (c) $V_{0.6}Fe_{0.4}BO_3$. The inset to Fig. 1c shows the magnetization on a magnified scale.

The mixture of the initial components was placed in closed platinum crucibles having a volume of 100 $cm^3$ and was held at $T = 1000°C$ until the charge was diluted completely. Then the mixture was rapidly cooled to 800°C and held for 1 h.

Using this technology, we obtained crystals in the form of thin plates with a size of $4 \times 4$ mm and a thickness of about 0.1 mm, having a smooth and bright surface.

The $V_xFe_{1-x}BO_3$ samples with $x = 0.6$ were subjected to X-ray structural and chemical analyses; the former analysis revealed that the compound with a mixed composition has the same crystal lattice as the extreme compounds $VBO_3$ and $FeBO_3$, while the latter analysis confirmed the closeness of the concentration $x$ of the substituent ion to that laid during synthesis. X-ray diffraction measurements carried out at 77 K revealed that the compound does not experience any phase transition.

## 3. EXPERIMENTAL RESULTS

The temperature and magnetic-field dependences of magnetization were measured with the help of a vibrating-coil magnetometer with a superconducting solenoid. Resistive measurements were made by a direct two-contact method using a teraohmmeter. Indium contacts were deposited using the surface wetting effect, and the sample temperature was controlled by its blasting with a gaseous nitrogen or air jet in a flow cryostat. We also obtained optical absorption spectra in the spectral region 4000–20 000 $cm^{-1}$ in the temperature range 83–300 K.

The results of complex measurements showed that, in the concentration range $0 < x < 0.5$, the magnetic and electrical properties of solid solutions are close to those of the initial compound $FeBO_3$. Figure 1a shows by way of an example the temperature dependences of magnetization for $FeBO_3$ (curve *1*) and for a composition with $x = 0.5$ (curve *2*) in a magnetic field of 10 kOe. Since $FeBO_3$ is a well-studied compound, it was not investigated additionally in the present work, and the data of magnetization of $FeBO_3$ were borrowed from [4]. Surprisingly, both curves exhibit the same behavior and demonstrate close values of magnetic moment at $T = 4.2$ K in spite of the fact that half iron atoms are replaced by vanadium atoms. However, the value of $T_N$ for the solid solution is considerably (approximately by 20 K) lower than for the initial compound.

While solid solutions remain close to $FeBO_3$ in the magnetic and electric respect in a wide concentration range of the substituent ion $V^{3+}$, the addition of small amounts of Fe to $VBO_3$ leads, on the contrary, to a rapid change in the nature of magnetic ordering. Although the curves describing the temperature dependence of magnetization for $VBO_3$ (curve *1*) [1] and for a composition with 5% Fe (curve *2*) have the same form typical of ferromagnets (Fig. 1b), the saturation magnetic moment for the solid solution at $T = 4.2$ K is 15% lower than for $VBO_3$.

For values of $x = 0.6$ and 0.75, the temperature dependences of magnetization are close and exhibit a

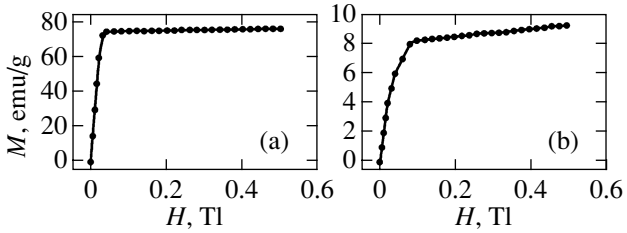


**Fig. 2.** Magnetization curves at $T$ = 4.2 K for (a) $V_{0.95}Fe_{0.05}BO_3$ and (b) $V_{0.6}Fe_{0.4}BO_3$.

complex behavior. Figure 1c shows the temperature dependence of magnetization for a $V_{0.6}Fe_{0.4}BO_3$ sample. It can be seen from the figure that the function $M(T)$ decreases near $T_C$, which is typical of pure $VBO_3$, but the value of the saturation magnetization $M_s$ amounts to only 10% of its value for the initial compound [1], although the vanadium concentration in the sample is 60%. In the vicinity of $T$ = 150 K, the curve has a peak followed by a decay in $M(T)$, which also displays singularities. Such an unusual behavior of $M(T)$ was observed in [4, 5] for solid solutions of $Cr_xFe_{1-x}BO_3$ and was attributed to the existence of an intermediate magnetic structure.

Figure 2 shows the $M(H)$ curves at $T$ = 4.2 K. It can be seen that the magnetization processes are different for samples with different compositions. For example, the tangent to the $M(H)$ curve in the region of strong fields for a sample with $x$ = 0.95 is almost parallel to the abscissa axis (Fig. 2a). The samples with $x$ = 0.5 are characterized by a weak paraprocess, while this process for an intermediate composition with $x$ = 0.6 and 0.75 is strong (Fig. 2b).

As regards the electric properties of the samples, the samples with $0 < x < 0.5$ are insulators (see above), while the remaining compositions, which are closer to $VBO_3$, are conductors whose resistivity decreases by 9% upon an increase in temperature from 77 to 550 K. The electric properties of samples with $x$ = 1 and 0.95 as well as of compositions with $x$ = 0.6 and 0.75 are close; for this reason, Fig. 3 depicts only the dependences for the former compositions. It can be seen from Figs. 3a and 3b that the temperature dependence of the resistance of $VBO_3$ is close to a simple activation law with the activation energy $E_a$ = 0.9 eV. At high temperatures, the composition $V_{0.6}Fe_{0.4}BO_3$ also displays activation conduction with a slightly higher value of $E_a$ = 1.1 eV. However, at lower temperatures, the linear dependence of $\ln R$ on reciprocal temperature is violated for this composition. It can be seen in Fig. 3c that, in this temperature range, the resistance is described more correctly by the law [6]

$$R \propto \exp(Q/k_BT)^{1/4},$$

where $Q$ is the quantity determined by the density of states at the Fermi level and by the rate of the decrease for the envelope of the wave function. This law is typical of hopping conduction with a varying jump length. Thus, this mechanism obviously dominates at low temperatures. Unfortunately, we cannot trace the concentration dependence of the absolute value of resistance for various samples since its variations are not very pronounced and the resistance cannot be measured pre-

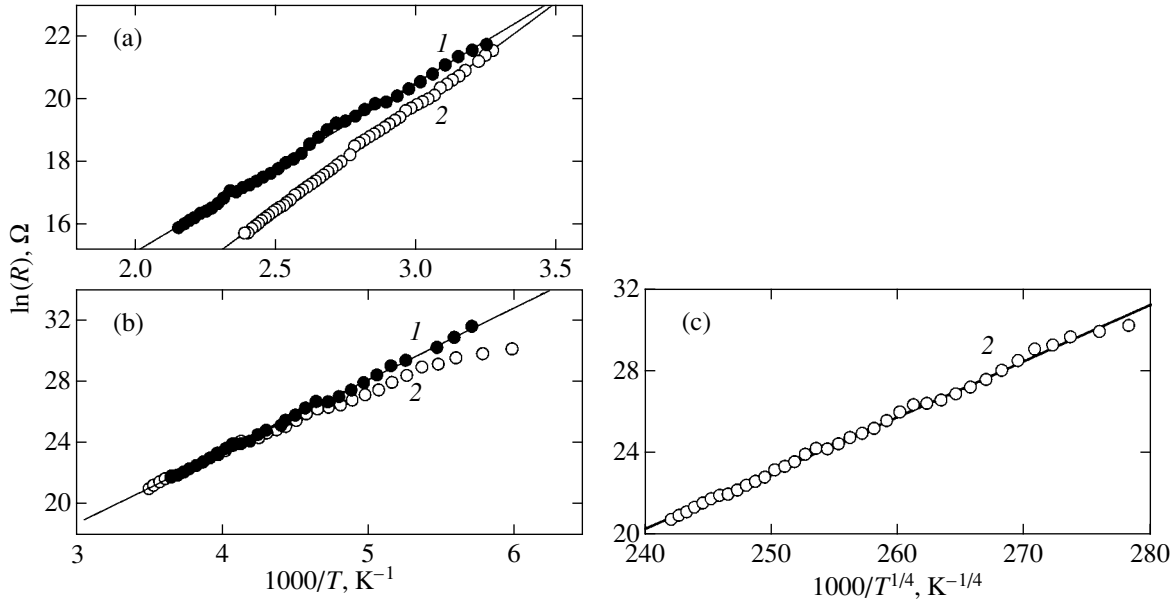


**Fig. 3.** Logarithm of resistance as a function of (a, b) reciprocal temperature 1000/$T$ and (c) 1000//$T^{1/4}$ for $VBO_3$ (*1*) and $V_{0.6}Fe_{0.4}BO_3$ (*2*) at (a) $T$ > 300 K and (b, c) $T$ < 300 K.

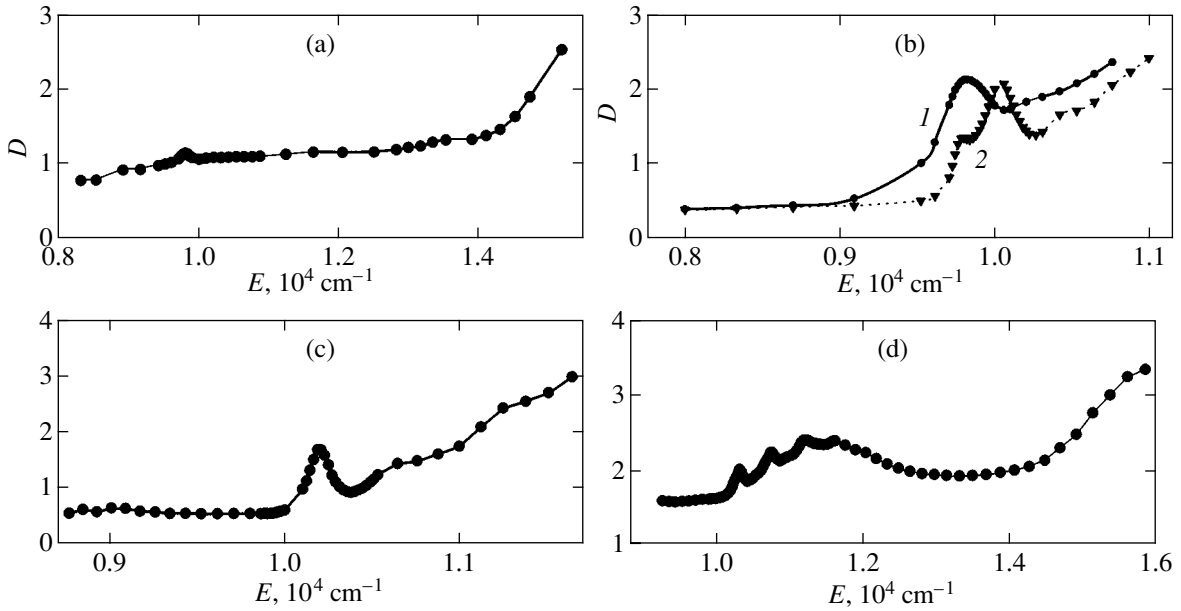


**Fig. 4.** Optical absorption curves at $T = 90$ K: (a) $VBO_3$; (b) $V_{0.75}Fe_{0.25}BO_3$ (curves *1* and *2* correspond to 300 and 90 K, respectively); (c) $V_{0.5}Fe_{0.5}BO_3$; and (d) $V_{0.25}Fe_{0.75}BO_3$.

cisely in view of the irregular geometrical shape of the samples.

The observed variation of the optical absorption spectrum $D = \ln(I_0/I)$ with $x$ is also nontrivial by nature. Figure 4 shows the spectral characteristics for samples from the series $V_xFe_{1-x}BO_3$. For the $VBO_3$ crystal (Fig. 4a), an extremely weak temperature-independent peak can be seen at 9800 $cm^{-1}$. The absorption edge corresponds to approximately 16 000 $cm^{-1}$. For a $V_{0.75}Fe_{0.25}BO_3$ crystal (Fig. 4b), the absorption edge is strongly displaced to 11 000 $cm^{-1}$. In addition to the 9800-$cm^{-1}$ peak typical of $V^{3+}$, a new peak with a clearly manifested temperature dependence appears. For a $V_{0.5}Fe_{0.5}BO_3$ sample (Fig. 4c), this peak remains, while the peak typical of $V^{3+}$ vanishes. Figure 4d shows the absorption spectrum for a $V_{0.25}Fe_{0.75}BO_3$ sample, which obviously contains a series of bands typical of $FeBO_3$ [7]. In all publications devoted to the absorption spectra of $FeBO_3$ (see, for example, [8]), this series of bands is attributed for phonon–magnon repetitions of the lowest–frequency transition ${}^6A_{1g} \longrightarrow {}^4T_{1g}$ in $Fe^{3+}$. Thus, the temperature-dependent absorption peak observed near 10 000 $cm^{-1}$ for intermediate concentrations of V and Fe cannot be attributed to single-ion transitions in $V^{3+}$ and $Fe^{3+}$.

Apart from the emergence of the additional absorption peak, the nonmonotonic change in the position of the fundamental absorption band edge is also nontrivial: with decreasing $x$, the edge is displaced to the long-wave region, but as $x$ approaches zero, it is abruptly shifted to the short-wave region as in the case of $FeBO_3$.

## 4. ONE-ELECTRON CALCULATIONS OF $FeB_6O_6$ AND $VB_6O_6$ CLUSTERS

In order to explain qualitatively the obtained experimental results, the knowledge of the electron structure is essential. Since borates (like other oxide dielectrics with localized *d* electrons) belong to the class of systems with strong electron correlations, the standard one-electron band calculations using the density functional method in the local dipole approximation (LDA) are inapplicable. In this situation, *ab initio* one-electron calculations of molecular orbitals (MO) for finite clusters provide incomplete, but rather valuable, information on the degree of hybridization of various cation and anion orbitals, the parameters of their splitting in the crystal field, and dipole matrix elements for interband transitions. In spite of the fact that the absolute values of electron energies cannot be correct if we disregard strong correlations, their difference can be rightfully used for a qualitative analysis of experimental data.

An analysis of the electron structure of the given compounds was carried out using the Hartree–Fock method with the help of the GAMESS package [9]. In view of the absence of metallic properties in both compounds, cluster methods of calculations could be applied. The necessity of taking into account the exchange effects exactly in order to explain the magnetic properties of Fe and V ions dictated the application of the Hartree–Fock method.

As a model, we chose the $FeB_6O_6$ ($VB_6O_6$) cluster (Fig. 5). The central Fe (V) atom is surrounded by an octahedron of oxygen atoms. In view of the small separation (1.42 Å) between the oxygen and boron atoms and strong hybridization of their orbitals, the boron

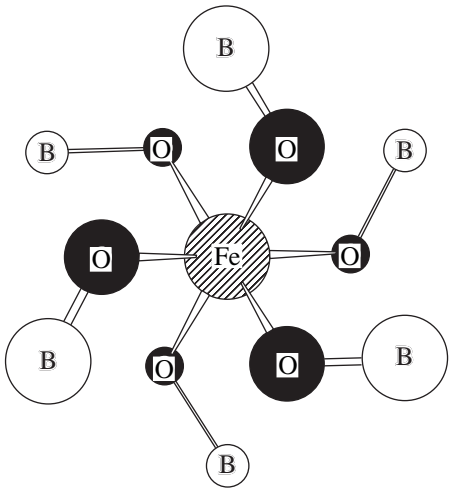


**Fig. 5.** Structure of the $FeB_6O_6$ ($VB_6O_6$) cluster being calculated.

atoms in the cluster had to be taken into account also. The chosen formula $Fe(V)B_6O_6$ of the cluster correctly describes the surroundings of the central metal atom in the first and second coordination spheres. In our calculations, we included the *s*, *p*, and *d* electrons of the cation; the *s* and *p* electrons of oxygen; and the *s* and *p* electrons of boron.

Since the effect of atoms from the next coordination spheres is disregarded in all cluster models, an additional charge *dZ* must be introduced into the cluster charge or *dZ* must be subtracted from the cluster charge. We chose the charge of the cluster under investigation equal to –3, since each boron atom has only one bond (with oxygen atoms), which corresponds to approximate occupancy of the *d* shell of the central atom of the metal.

The calculations for $VB_6O_6$ (even number of electrons) and for $FeB_6O_6$ (odd number of electrons) were carried out for a triplet and for a doublet, respectively. According to the results of calculations, the level corresponding to the highest occupied molecular orbital (HOMO) is formed by the *d* shell of the Fe (V) atom, which is weakly hybridized with other orbitals of the cluster. This is visually shown in Fig. 6 depicting the partial densities of states for both compounds. In these figures, the contributions from the *s*, *p*, and *d* electrons of the central metal atom; the *sp* shells of oxygen; and the *sp* shells of boron are presented successively from bottom to top. It can be seen that the *d* level for Fe lies much lower on the energy scale than in the shell of the V atom. This shift is apparently associated with the larger charge of the nucleus of the Fe atom, which lowers the energy of the *d* electron.

For both crystals, a weak *sp*–*d* hybridization of the *d* electrons of the cation and the *sp* states of the anion is observed. For $VB_6O_6$, a very small addition to the density of states from the 3*d* electrons can be seen in the energy range 1.1–1.3 eV, where the contributions from the *p*(V), *p*(O), *s*(B), and *p*(B) atomic orbitals dominate. In the HOMO region, one can see a very small contribution from the *p* orbitals of oxygen. The splitting of the HOMO peaks for $VB_6O_6$ by $\Delta E \approx 0.4$ eV corresponds to the splitting of the electron $t_{2g}$ level due to the uniaxial crystal field component. For $FeB_6O_6$, the *p*–*d* hybridization is stronger than for vanadium, which is manifested in the larger height of the *d* peak of Fe in the partial density of states with an energy of 1.3 eV and the peak of the *d* states of oxygen in the HOMO. At the same time, strong hybridization of the *s* and *p* states of the cation with the *p* states of oxygen and *sp* states of boron takes place for both compounds; this hybridization determines the covalent component of the chemical bond as well as the optical absorption spectra.

The calculated energy levels and dipole matrix elements formed the basis for simulating the optical absorption spectra (Fig. 7). It can be seen that the absorption spectra for these compounds are completely

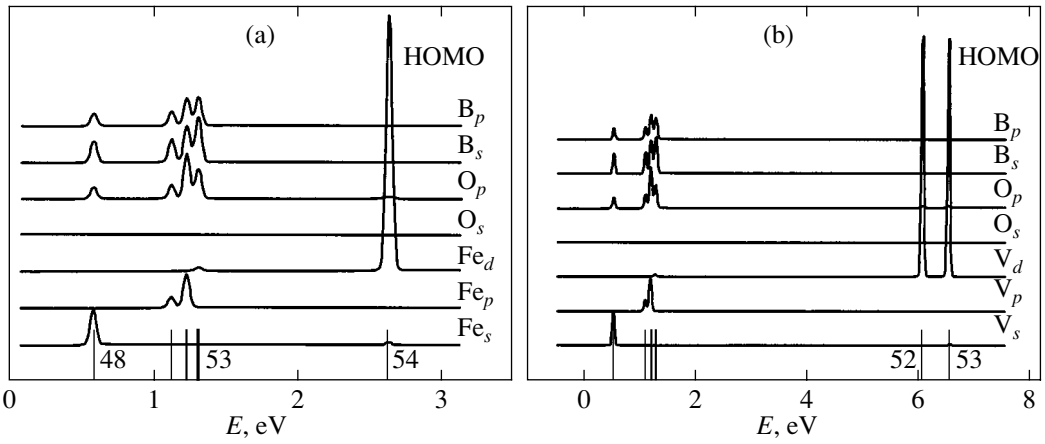


**Fig. 6.** Partial density of states for (a) $FeB_6O_6$ and (b) $VB_6O_6$ clusters. The lower scale shows the energy levels of molecular orbitals.

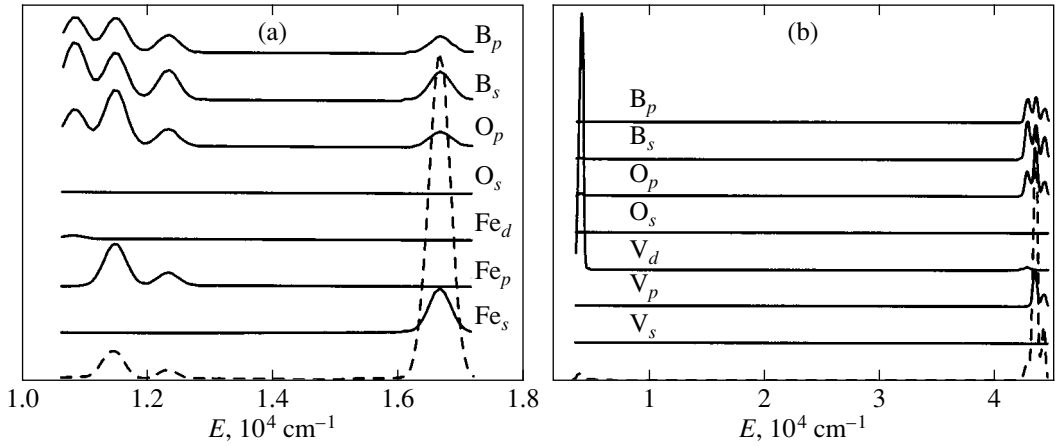


**Fig. 7.** Combined partial density of states relative to the HOMO level (solid curves) and optical absorption (dashed curves) for (a) $FeB_6O_6$ and (b) $VB_6O_6$ clusters.

different due to different positions of the *d* shell of the metal relative to other shells.

It can be seen from Fig. 7 that the optical absorption spectrum is determined by the dipole transitions from filled MO to partly filled HOMO. For $FeB_6O_6$, three absorption peaks repeating qualitatively the absorption spectrum of $FeBO_2$ [7] are observed in the energy range $(10–16) \times 10^3$ cm$^{-1}$: closely spaced peaks in the range $(1.1–1.25) \times 10^4$ cm$^{-1}$ (Fig. 7a) correspond to the broad absorption peak for a $FeBO_3$ crystal with the center at $1.15 \times 10^4$ cm$^{-1}$, while the position of the peak at $1.65 \times 10^4$ cm$^{-1}$ completely coincides with the experimental peak. Naturally, various types of interactions occurring in the crystal may lead to a renormalization of the spectrum. In view of the absence of fitting parameters in the calculations and the simplicity of the $FeB_6O_6$ cluster, we may conclude that the main contribution to partial densities of states and to the optical spectra is formed by the electron bonds in the first and second coordination spheres.

For $VB_6O_6$, high-intensity p–*d* transitions from the filled MO to the partly filled HOMO produce a high-intensity peak with an energy exceeding $4 \times 10^4$ cm$^{-1}$, which is beyond the range of our measurements. Weak *d*–*d* transitions allowed due to the cation–anion *p*–*d* hybridization lead to a low-intensity peak at 9800 cm$^{-1}$. A theoretical analysis leads to a similar low-intensity peak with the energy $\Delta E = 0.4$ eV, presented in Fig. 7b, which is determined by the splitting of the filled (band index $\lambda = 1$) and unfilled ($\lambda = 2$) parts of the $t_{2g}$orbitals in the crystal field. In this case, the intra-atomic Coulomb interaction between different orbitals in the $t_{2g}$ configuration enhances this splitting. Indeed, the Hamiltonian of such an interaction can be written in the form

$$H^{12} = \varepsilon_1 n_{d1} + \varepsilon_2 n_{d2} + V_{12} n_{d1} n_{d2}, \qquad (1)$$

where $n_{d\lambda} = \sum c^{+}_{d\lambda\sigma} c_{d\lambda\sigma}$ is the operator of the number of *d* electrons at the $\lambda$ level; $c_{d\lambda\sigma}$ is the annihilation operator for a *d* electron at the $\lambda$ level with spin $\sigma$; and $\varepsilon_1$, $\varepsilon_2$, and $V_{12}$ are the energies of molecular orbitals 1, 2 and the parameter of the Coulomb interaction between them. In the simplest mean-field approximation,

$$V_{12} n_{d1} n_{d2} \longrightarrow V_{12} n_{d1} \langle n_{d2} \rangle + V_{12} \langle n_{d1} \rangle n_{d2},$$

we obtain renormalized MO levels,

$$\tilde{\varepsilon}_1 = \varepsilon_1 + V_{12} \langle n_{d2} \rangle, \quad \tilde{\varepsilon}_2 = \varepsilon_2 + V_{12} \langle n_{d1} \rangle, \qquad (2)$$

and the transition energy

$$\Delta \tilde{E} = \varepsilon_2 - \varepsilon_1 + V_{12} (\langle n_{d1} \rangle - \langle n_{d2} \rangle). \qquad (3)$$

Since orbital 1 is filled ($\langle n_{d1} \rangle = 1$) and orbital 2 is empty ($\langle n_{d2} \rangle = 0$), the line in the absorption spectrum is determined not only by the splitting $\Delta E = \varepsilon_2 - \varepsilon_1$ in the crystal field, but also by the Coulomb interorbital matrix element. Considering that the typical value of $V_{12}$ for 3*d* metal oxides is on the order of 1 eV, we obtain the shift of the theoretical peak depicted in Fig. 7b to the region of observable values.

## 5. DISCUSSION

The most adequate model of the electron structure of 3*d* metal borates, which describes the electric and magnetic properties on a unified basis, is the multiband Hubbard model taking into account different *d* orbitals explicitly as well as their interatomic overlapping and strong electron correlations $U \gg t$, where *t* is the jump integral. In this model, $FeBO_3$ with the $3d^5$ configuration for the $Fe^{3+}$ ion is an analogue of the conventional orbital-nondegenerate Hubbard model with a half-filled band, in which the indirect exchange interaction $J \sim t^2/U$ through anions is of the antiferromagnetic type.

For $VBO_3$ with the $d^2$ configuration of the $V^{3+}$ ion, we have one unfilled orbital in the $t_{2g}$ shell, which, in the language of the Hubbard model, leads to a kinematic ferromagnetic exchange interaction. The separation between filled and unfilled $t_{2g}$ orbitals (3) determines not only the peak in the optical absorption spectrum, but also the conduction activation energy $E_a \approx 0.9$ eV.

In solid solutions $V_xFe_{1-x}BO_3$, the average number of $d$ electrons per cation is

$$n_d = 5(1-x) + 2x = 5 - 3x. \quad (4)$$

For a low Fe concentration in the range $2/3 < x < 1$, charge carriers are holes in $t_{2g}$ states, which ensure the semiconductor-type conduction. The concentration $x_c = 2/3$ is critical in the sense that it corresponds to half the filling of the $t_{2g}$ levels, i.e., to the $t_{2g}^3$ configuration. Considering that the $e_g$ levels of $d$ electrons lie above the $t_{2g}$ levels by the cubic crystal field component, $10D_q \approx 3$–$5$ eV, we arrive at the conclusion that the $t_{2g}^3$ configuration is analogous to a half-filled band in the one-band Hubbard model, and strong electron correlations lead to the localization of charge carriers. Thus, a transition from the semiconductor-type conduction to the dielectric state occurs at concentration $x = x_c$. In view of composition disorder in solid solutions, the temperature dependence of the resistance near $x_c$ at low temperatures is of the characteristic Mott type $\ln R \propto T^{1/4}$ corresponding to jumps with a varying jump length (see Fig. 3). As regards the magnetic properties, an additional integral of indirect exchange through the anions, which is responsible for the antiferromagnetic contribution as in the Hubbard model and for the additional scale in Fig. 1c, appears in the case of the half-filled $t_{2g}^3$ configuration. The approach described above corresponds to an averaged pattern. In the nonaveraged form, we can speak of the exchange integrals $I(V^{3+}$–$V^{3+})$ (ferromagnetic), $I(Fe^{3+}$–$Fe^{3+})$ (antiferromagnetic), and $I(V^{3+}$–$Fe^{3+})$ (antiferromagnetic). For $x \approx 0.5$ (including the range of $x \sim x_c$), the number of $V^{3+}$–$Fe^{3+}$ pairs is maximum, and it is the interaction between such pairs which is apparently manifested in the form of the peak at $T = 150$ K (Fig. 1c).

In the other limiting case of a low vanadium concentration, the electron structure is determined by a superposition of the $d^5$ and $d^4$ configurations. The role of charge carriers may probably be played by holes from the $e_g$ shell, but they are localized due to the small band width in view of weak cation–anion hybridization.

In order to interpret the optical absorption spectra in solid solutions, we calculate the spectrum of a virtual crystal consisting of independent absorbing $FeBO_3$ and $VBO_3$ centers using the formula

$$D(x) = xD(VBO_3) + (1-x)D(FeBO_3), \quad (5)$$

where the $D(VBO_3)$ and $D(FeBO_3)$ spectra are taken from the experimental data for the initial single crystals (Fig. 8).

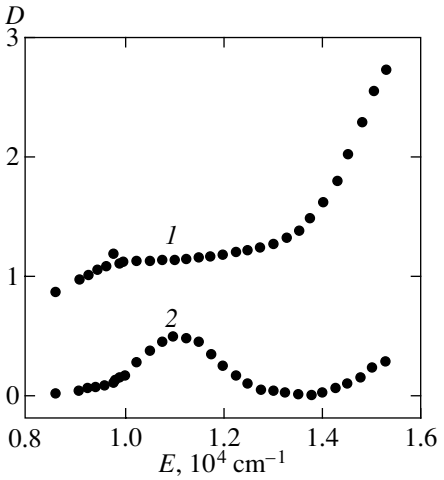


**Fig. 8.** Experimental absorption spectra for $VBO_3$ (*1*) and $FeBO_3$ (*2*) at $T = 300$ K.

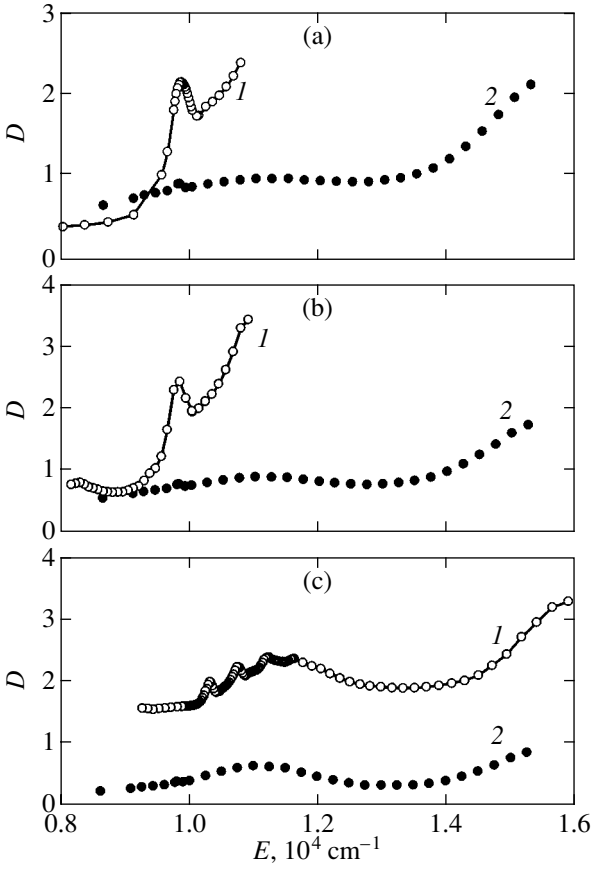


**Fig. 9.** Absorption spectra for (a) $V_{0.75}Fe_{0.25}BO_3$, (b) $V_{0.6}Fe_{0.4}BO_3$, and (c) $V_{0.25}Fe_{0.75}BO_3$: experimental curves *1* were obtained at $T = 300$ K (a, b) and $T = 90$ K (c); theoretical curves *2* correspond to $T = 300$ K.

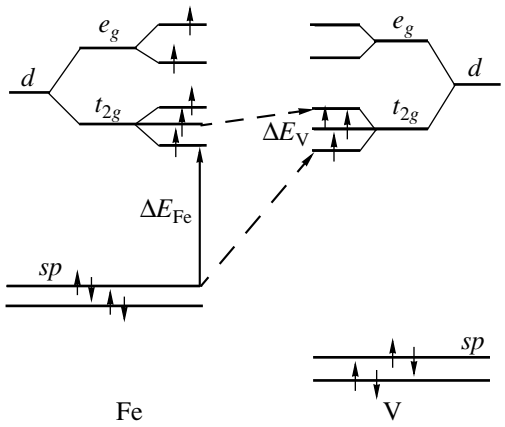


**Fig. 10.** Diagrams of molecular orbitals for $FeBO_3$ and $VBO_3$.

The experimental spectra with those calculated on the basis of formula (5) for the compositions $V_{0.75}Fe_{0.25}BO_3$, $V_{0.6}Fe_{0.4}BO_3$, and $V_{0.25}Fe_{0.75}BO_3$ are compared in Figs. 9a, 9b, and 9c, respectively. It can be seen from the figure that the positions of the experimental peaks are close to the corresponding peaks for the initial components, but the peak intensities are much higher than for the virtual crystal. The reason for the increase in the peak intensity is explained in Fig. 10 showing the diagrams of molecular orbitals for $FeBO_3$ and $VBO_3$, constructed on the basis of the numerical calculations of clusters in Section 4. The notation in the figure corresponds to the initial atomic orbitals of *d* electrons of the cation and the *sp* electrons of oxygen and boron; actually, molecular orbitals with small admixtures of states due to the *sp*–*d* hybridization are presented. Here, $\Delta E_{Fe}$ and $\Delta E_V$ are the energies of transitions between molecular orbitals of $FeBO_3$ and $VBO_3$, determining the absorption peaks at 11 000 and 9800 $cm^{-1}$, respectively. In addition to independent contributions to the spectrum in a solid solution (formula (5)), a mutual effect takes place when the unit cells of $FeBO_3$ and $VBO_3$ occupy neighboring positions. This effect is manifested in the enhancement of the *sp*–*d* hybridization, since the *sp* states of boron and oxygen belong simultaneously to the $FeBO_3$ and $VBO_3$ cells. This gives rise to additional optical transitions with energies $\Delta E_{Fe}$ and $\Delta E_V$, which are depicted in Fig. 10 by inclined dashed lines and are responsible for the enhancement of peaks in the absorption spectrum as compared to the virtual crystal.

## ACKNOWLEDGMENTS

The authors are grateful to A. F. Bovina who carried out X-ray measurements.

This work was supported by the Russian Foundation for Basic Research (project no. 99-02-17405).

## REFERENCES

1. T. A. Bither, C. G. Frederick, T. E. Gier, *et al.*, Solid State Commun. **8**, 109 (1970).
2. H. Schmid, Acta Crystallogr. **17**, 1080 (1964).
3. B. Andlauer, J. Schneider, and W. Wettling, Appl. Phys. **10**, 189 (1976).
4. O. Müller, M. P. O'Horo, and J. F. O'Neill, J. Solid State Chem. **23**, 115 (1978).
5. M. P. O'Horo and O. Müller, J. Appl. Phys. **49**, 1516 (1978).
6. N. F. Mott, *Metal-Insulator Transitions* (Taylor & Francis, London, 1974; Nauka, Moscow, 1979).
7. V. N. Zabluda, A. V. Malakhovskiĭ, and I. S. Édel'man, Fiz. Tverd. Tela (Leningrad) **27**, 133 (1985) [Sov. Phys. Solid State **27**, 77 (1985)].
8. B. Andlauer, O. F. Schirmen, and J. Schneider, Solid State Commun. **13**, 1655 (1973).
9. M. W. Schmidt, K. K. Balridge, J. A. Boats, *et al.*, J. Comput. Chem. **14**, 1347 (1993).

*Translated by N. Wadhwa*